

<https://doi.org/10.1038/s42003-025-08314-2>

Differential regulation of mTOR activity in retinal ganglion cells underlies their distinct susceptibility to ischemia/reperfusion

Meizhen Zhu¹, Yuqing Wu¹, Hang Gao^{1,2}, Fujian Qi³, Xiaoyu Zhang¹ & Yanli Ran¹

Retinal ischemia/reperfusion (I/R) injury drives progressive retinal ganglion cell (RGC) loss, yet mechanisms underlying neuronal type-specific vulnerability remain unclear. Using a mouse model of bilateral common carotid artery ligation, we observe decreased vessel density in the inner retina following I/R. Here, the total RGCs exhibit much more cell loss than the intrinsic photosensitive RGCs (ipRGCs). This disparity is parallel with their different mTOR activity: for ipRGCs, the mTOR activity is much higher than the total RGCs both before and after I/R. Pharmacological experiments reveal that, mTOR activation in total RGCs and high mTOR activity maintenance in ipRGCs promote rapamycin to protect the total RGCs and ipRGCs against I/R injury, respectively. Notably, the protective effects of rapamycin on total RGCs and ipRGCs manifest under different light conditions. Our findings bridge the type-specific mTOR regulation in RGCs and their distinct susceptibility to I/R injury, which offers new insights into further targeted neuroprotection.

Retinal I/R injury results from an insufficient supply of blood flow, characterized by excitotoxicity, inflammation, cell death and vision impairment. I/R injury is associated with various ocular diseases, such as glaucoma, diabetic retinopathy and retinal vascular occlusion¹. After I/R, damage to the retina is often inhomogeneous, with the inner retina showing more cell loss, especially RGCs, which are particularly vulnerable to I/R^{2–4}. RGCs serve as the output neurons of the retina, transmitting all information processed by retinal circuits to the brain. Damage to RGCs directly impair the visual pathway. Therefore, it is crucial to prevent the functional loss and death of RGCs in treating various ophthalmic diseases.

One critical factor influencing cell fate after ischemia is the mammalian target of rapamycin (mTOR), which is highly sensitive to energy supply and regulates essential cellular processes such as cell viability and apoptosis^{5–7}. In the context of ischemic excitotoxicity, activating N-methyl-D-aspartate receptors (NMDARs) can lead to the downregulation of mTOR activity^{8–10}. Some studies in animal models have demonstrated that upregulation of mTOR activity has beneficial effects on the damaged tissue, which reduces glutamate excitotoxicity and neuronal impairment^{11–13}. Conversely, other studies suggest that inhibiting mTOR activity offers protective effects against ischemic damage in neurons^{8,14–16}. These discrepancies may arise from the fact that most studies

have measured overall mTOR activity at the tissue level without distinguishing between different cell types. As a result, the contradictory findings could be attributed to varying responses across different cell populations. So far, whether different cell types vary in their ability to maintain mTOR activity and how this relates to their susceptibility to I/R still remain to be elusive.

In the mammalian retina, there are more than 30 RGC types, each exhibiting distinct physiology and function^{17–19}. Herein, the ipRGCs, accounting for a small population of RGCs, which express melanopsin, compared with other RGC types, have been reported to show higher resistance to ocular injuries, such as optic nerve crush^{20–23} and glaucoma^{24,25}. These cells have also been recently reported to be resistant to NMDA-induced excitotoxicity²⁶, suggesting a potential high resistance to I/R-induced excitotoxicity. We hypothesized that the regulation of mTOR activity varies among RGC types with differential susceptibility to I/R. In this study, we demonstrate that ipRGCs are more resistant to I/R injury and maintain higher mTOR activity compared with total RGCs. The cell decreases in both total RGCs and ipRGCs following I/R can be alleviated by rapamycin administration, which suppresses the overall mTOR activity while either promoting mTOR activity in total RGCs or maintaining high mTOR activity in ipRGCs. The protective effects of rapamycin on total

¹Key Laboratory of Preclinical Study for New Drugs of Gansu Province, and Institute of Physiology, School of Basic Medical Sciences, Lanzhou University, Lanzhou, China. ²School of Public Health, Lanzhou University, Lanzhou, China. ³School of Life Sciences, Lanzhou University, Lanzhou, China.

e-mail: ranyl@lzu.edu.cn

RGCs and ipRGCs and the accompanied high mTOR activity manifest under different light conditions. Together, our findings raise the possibility of cell-type-specializations in their responses to I/R injury and mTOR regulations, and provide a potential intracellular link between neural activity and neuron protection against damage.

Results

Inhomogeneous effects of I/R on different retinal layers

To assess the effects of I/R on the retina, we constructed a standardized global I/R model in mice through bilateral common carotid artery ligation (BCAL) for the induction of retinal ischemia and subsequent reperfusion. The retina I/R was confirmed and estimated through in vivo imaging using optical coherence tomography angiography (OCTA; Fig. 1). After BCAL, the retinal blood flow was seriously blocked, which induced the swelling of the inner retina (Fig. 1A, B). Although blood flow was re-perfused and the swollen inner retina recovered when the ligation was removed, the supply of blood flow was not as sufficient as pre-BCAL. To quantitatively measure the recovery extent of blood flow after reperfusion, we analyzed the vessel densities based on their brightness after reperfusion. We found that the percentage of bright vessels did not change significantly after I/R within 7 days except for the inner retina (Fig. 1C). Both in the GCL and IPL, the density of bright vessels decreased dramatically on the 7th day of I/R (Fig. 1C). For the IPL, this decrease presents significance at the 3rd day of I/R. The changes in the density of bright vessels were not associated with the retinal thickness alterations (Fig. 1D).

The density reduction of bright vessels acquired from OCTA images could be due to a lack of perfusion or vascular density changes. To verify this, we analyzed the vessel density by IB4 staining in the fixed whole-mount retina (Fig. 2). The IB4 staining results showed that the vessel density in the superficial layers dropped especially fast from the 1st day to the 3rd day of I/R, and much slower afterwards, resulting in a significant vessel density decrease from the 3rd day of I/R. This is in line with the density change of bright vessels acquired from the OCTA recordings, revealing that I/R induces vessel density decrease in the inner retina, which can potentially initiate a series of neurotoxic cascades and subsequently lead to neurodegeneration.

Retina ganglion cell loss after I/R

The deficient supply of blood flow can rapidly lead to neurodegeneration and cell loss. To probe the effects of I/R on RGCs, we counted RGC numbers in the whole-mounted retina after immunostaining (Fig. 3A). For cell counting, we divided the retina into four quadrants and selected areas at different distances from the optic nerve. As previous studies reported that RGC distribution was not homogeneous across the mouse retina^{27–29}, our data showed that RGC density varied along the dorsal-ventral axis, with a slightly higher overall RGC density in the ventral retina (Fig. 3B, C). This asymmetric distribution of RGCs was maintained within 7 days after I/R. For both the dorsal and ventral retina, the significant decrease in RGC number was first observed on the 3rd day of I/R. Afterwards, there was only a slight decrease till the 7th day (Fig. 3D, E). Accordingly, RGC loss in the

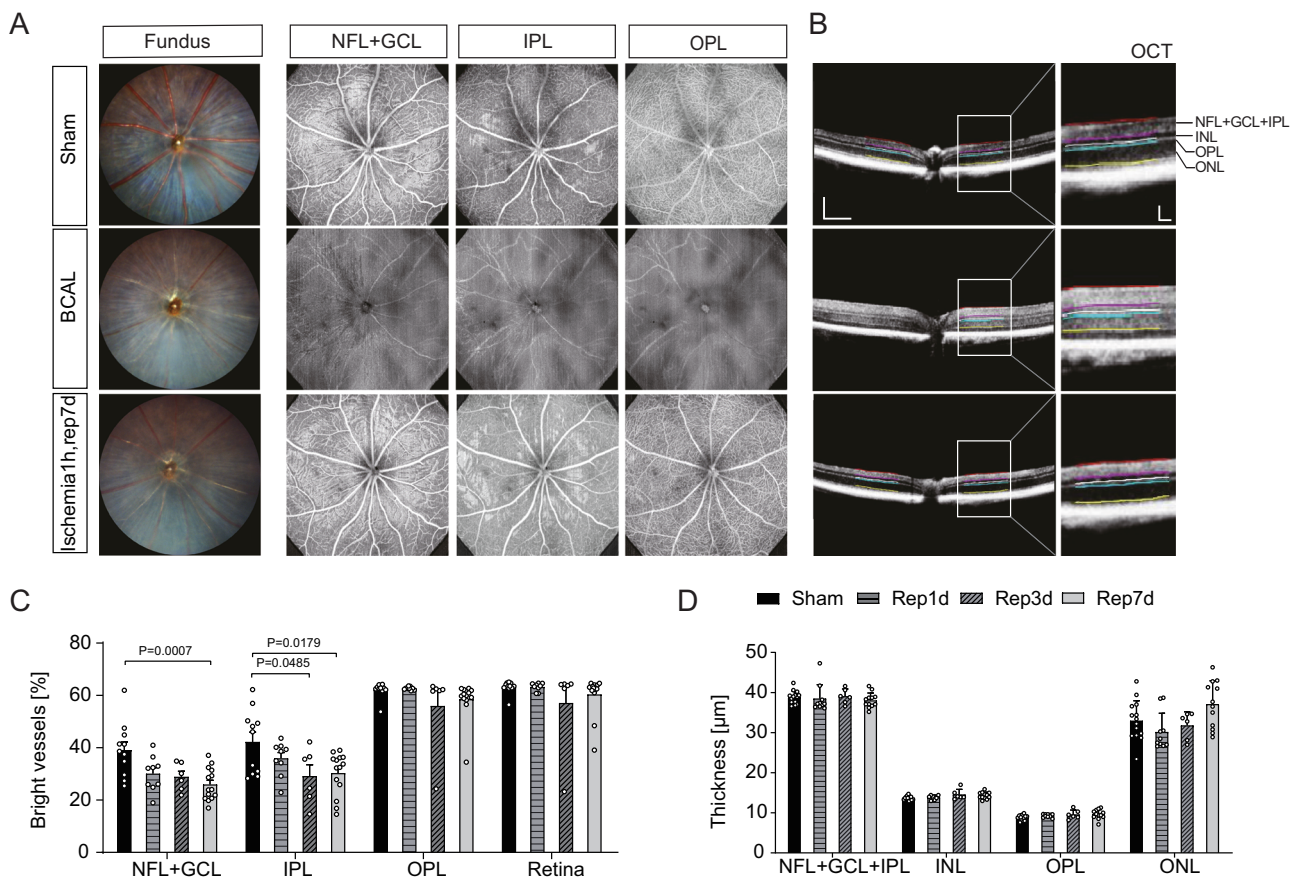


Fig. 1 | I/R leads to vascular alterations in the inner retinal layers. **A** Fundus images and OCTA images of the same eyeball from one mouse before ligation (Sham), after ligation (BCAL) and reperfusion 7 days, respectively. Left: Fundus images of retinal vessels; Right: Angiogram of retinal scans obtained through OCTA showing retinal NFL + GCL, IPL and OPL vessels. **B** Retinal tomography images from OCTA (scale bar: horizontal, 250 µm; vertical: 150 µm), with a magnified image on the right (scale bar: horizontal, 50 µm; vertical: 50 µm). **C** Percentage of

bright vessels of NFL + GCL, IPL, OPL and whole retina in the sham ($n = 11$ eyes, $n = 8$ mice), Rep1d ($n = 9$ eyes, $n = 5$ mice), Rep3d ($n = 6$ eyes, $n = 4$ mice) and Rep7d ($n = 14$ eyes, $n = 10$ mice) mice. * $p < 0.05$, *** $p < 0.001$. **D** Thicknesses of the inner retina (NFL + GCL + IPL), INL, OPL, and ONL in the sham ($n = 14$ eyes, $n = 7$ mice), Rep1d ($n = 10$ eyes, $n = 5$ mice), Rep3d ($n = 6$ eyes, $n = 4$ mice) and Rep7d ($n = 12$ eyes, $n = 9$ mice). Data were displayed as mean \pm SEM.

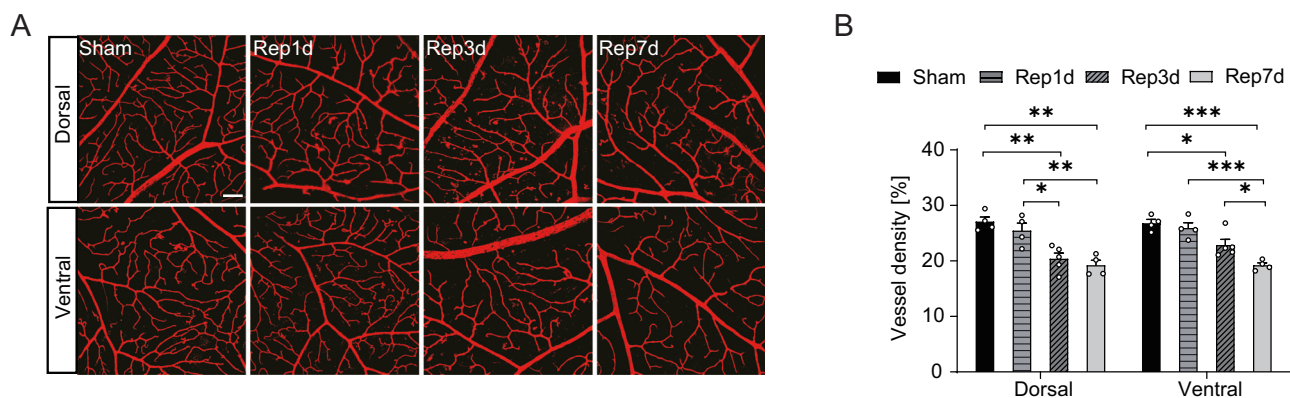


Fig. 2 | I/R reduces vascular density in the superficial retinal layer.

A Representative images showing blood vessels (IB4, red) in the surface capillary plexus of the flat-mounted retina in sham, Rep1d, Rep3d and Rep7d groups of mice. Scale bar: 50 μ m. **B** Statistic results of dorsal and ventral retinal vascular densities.

Sham: $n = 4$ eyes from 4 mice, Rep1d: $n = 4$ eyes from 4 mice, Rep3d: $n = 5$ eyes from 5 mice, Rep7d: $n = 4$ eyes from 4 mice. Data were displayed as mean \pm SEM.

* $p < 0.05$, ** $p < 0.01$, *** $p < 0.001$.

ischemic retina relative to that in retinas without ischemia was significant on the 3rd and 7th day of reperfusion (Fig. 3D, E). The RGC reduction between the dorsal and ventral retina was almost identical (Supplementary Fig. 1A). When comparing the RGC loss between the central and peripheral retina, we found that there was more RGC loss in the peripheral retina than the central retina (Fig. 3E, Supplementary Fig. 1B), which might be attributed by the different vasculature features in the central and peripheral retina. The reductions of RGC number across the retina were all significant on the 3rd day of I/R, which was aligned with the timeline of vessel density decrease in the inner retina, indicating that, for the ischemic retina in this study, the significant effects of I/R could be detected on the 3rd day of reperfusion. Therefore, we investigated further these RGCs on the 3rd day of reperfusion.

Previous studies have reported different RGC types exhibit differential resistance to pathological damage, with some RGC types exhibiting high susceptibility while other RGC types present strong resistance. Therein, ipRGCs show resistance to various damage^{32,21–24}. We asked whether ipRGCs also exhibit resistance to I/R damage. To answer this question, we counted ipRGC numbers across the retina. The melanopsin staining showed more ipRGCs in the dorsal retina when compared with the ventral retina (Fig. 4A–C), consistent with that previously reported^{30,31}. Unlike the total RGC number and the vessel density changes following I/R, the number of ipRGCs showed no significant decrease till the 3rd day of reperfusion and only reduced in the dorsal retina till the 7th day of reperfusion (Fig. 4D, E). This decrease was still less than the total RGCs (rep7d: $21.72\% \pm 11.13\%$ in ipRGCs vs $32.97\% \pm 10.48\%$ in total RGCs), indicating the cell loss occurred in non-ipRGCs was much more than the ipRGCs. To directly test this, we analyzed the Brn3a+ RGC density after 3 days of I/R. Our data showed that I/R induced a remarkable density reduction in Brn3a+ RGCs, which was comparable to the density decrease of total RGCs (Supplementary Fig. 2). Therefore, these findings reveal that ipRGCs are more resistant to I/R damage than other RGCs. Notably, studies reported that the melanopsin expression was downregulated after injury^{32,33}, and thus, the ipRGC density after I/R might be even more than that we observed, hiding a greater tolerance to I/R than other RGCs.

Higher mTOR activity in ipRGCs compared with total RGCs

The differential cell loss between ipRGCs and non-ipRGCs following I/R inspires us to explore the intrinsic properties underlying their resistance to I/R injury. Previous studies have reported that one important determinant of the cell fate after I/R is mTOR activity^{5–7}. Therefore, we hypothesized that the high resistance of ipRGCs to I/R injury was due to the high mTOR activity in this RGC type. To test this hypothesis, we examined the levels of pS6 signal, an indicator of mTOR³⁴, in all RGCs, ipRGCs and non-ipRGCs before and after I/R. Within one week after I/R, the pS6 staining was densest at the 3rd day, increased about 2 folds compared with the retina without I/R

(Fig. 5A, B). Like the RGC number decreases, the pS6 expression showed no detectable differences between dorsal and ventral retina (Fig. 5C).

When analyzing the expression of pS6 in total RGCs, we found that pS6 expressing RGCs also increased significantly following I/R (Fig. 6A–C), which is in line with the total pS6 expression (Fig. 5). For ipRGCs, the number of pS6 expressing cells was not affected by I/R (Fig. 6D, E), this high pS6 expression was also maintained on the 7th day of I/R when ipRGCs showed cell loss (Supplementary Fig. 3). Notably, though ipRGCs are only a minor fraction of the total RGCs, about half of the pS6 expressing RGCs are ipRGCs (71.65 ± 10.54 cells/ mm^2 in total RGCs, 44.47 ± 2.44 cells/ mm^2 in ipRGCs, without I/R; 106.90 ± 12.04 cells/ mm^2 in total RGCs, 49.49 ± 9.14 cells/ mm^2 in ipRGCs, Rep3d; Fig. 6B, E), resulting in a much higher percentage of pS6 expressing cells in ipRGCs than total RGCs (Fig. 6C, F). Accordingly, the percentage of pS6 expressing cells in non-ipRGCs was much lower than ipRGCs both before and after I/R, though it significantly increased after I/R like the total RGCs (Supplementary Fig. 4). The different expression of pS6 between non-ipRGCs and ipRGCs suggests that the activation of mTOR in ipRGCs is more than the other RGCs and, that mTOR activation might contribute to the higher resistance of ipRGCs in the I/R retina.

Rapamycin promotes mTOR activation in RGCs and alleviates RGC loss following I/R

To investigate whether mTOR activation affects RGC survival following I/R, we administered rapamycin to inhibit mTOR activity. In ischemic retinas from mice with rapamycin treatment, the number of cells with high pS6 expression was significantly less than those without rapamycin administration, indicating rapamycin suppressed mTOR activity during retina I/R injury (Fig. 7A, B). However, the mTOR activities in RGCs increased in retinas from rapamycin-injected mice (Fig. 7C, D), with an increased pS6-positive RGCs (106.9 ± 12.04 cells/ mm^2 in vehicle vs 282.6 ± 66.77 cells/ mm^2 with rapamycin). The controversial effects of rapamycin on the total mTOR activity and mTOR activity in RGCs indicate that rapamycin-induced inhibition of mTOR activity mainly occurs in non-RGCs. Indeed, we found that with rapamycin administration, there was a pronounced decrease in pS6 expressing astrocytes (Supplementary Fig. S5). For the total RGCs, rapamycin led to an increased fraction of pS6 expressing cells, with $69.41\% \pm 4.71\%$ (Rapa) vs $16.05\% \pm 1.81\%$ (Vehicle) of the total pS6 positive cells. This increase mainly occurred in the non-ipRGCs (Supplementary Fig. 6). Unlike the total RGCs and non-ipRGCs, rapamycin dramatically decreased the number of pS6 expressing ipRGCs (Fig. 7E, F; Supplementary Fig. 7).

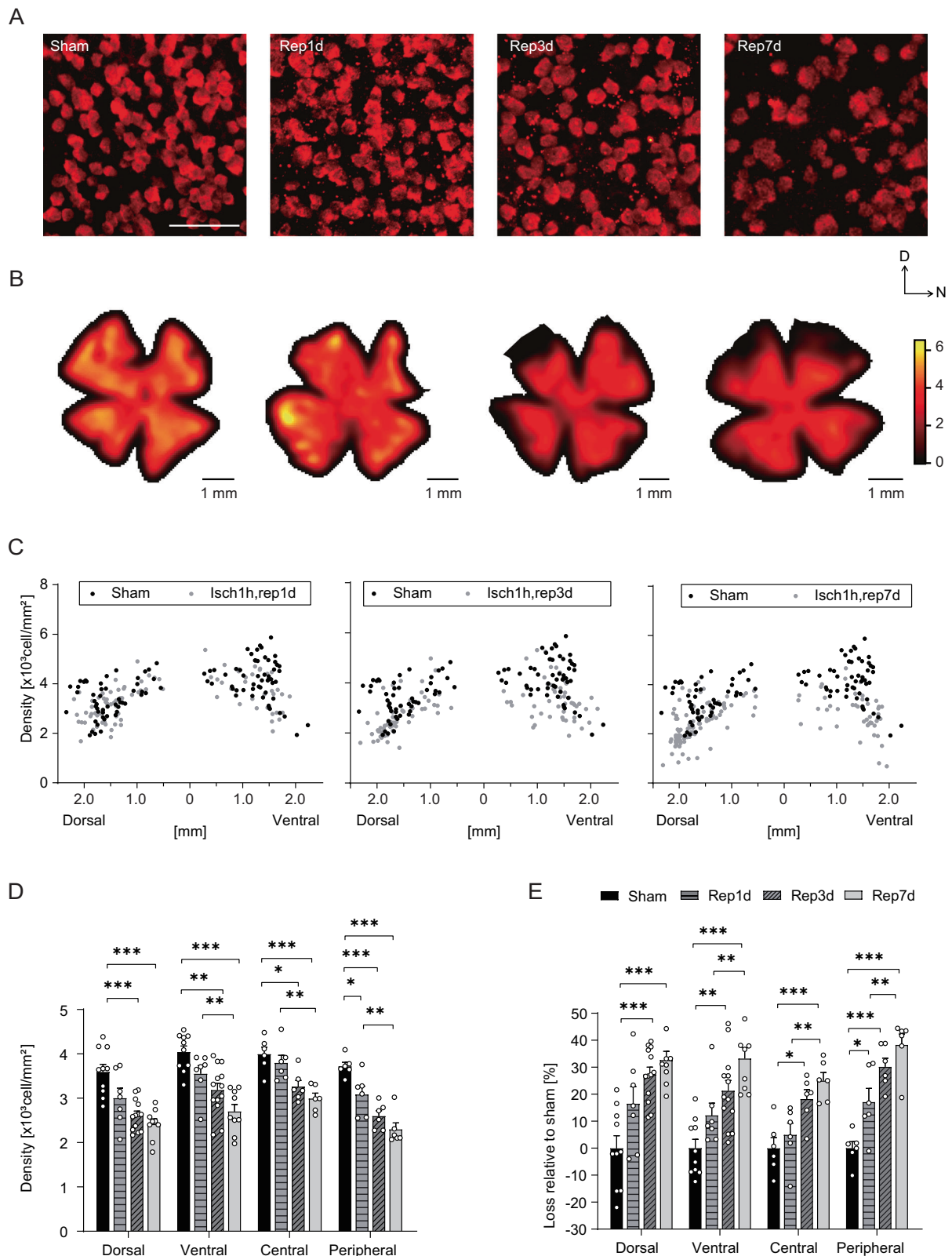


Fig. 3 | RGC loss within one week after I/R injury. **A** Representative images of RBPMS+ (red) immunostaining. Scale bar: 50 μm . **B** Densities of RBPMS+ RGCs across the whole retina. Color bar: cell number in areas of $60 \times 60 \mu\text{m}^2$. D: dorsal, N: nasal. **C** Scatter plots showing RGC density along the ventral-dorsal axis (horizontal axis with 0 for optic nerve). **D** Quantitative analysis of RBPMS+ cell density in the dorsal and ventral (Sham: $n = 10$ eyes from 5 mice, Rep1d: $n = 7$ eyes from 4 mice,

Rep3d: $n = 13$ eyes from 7 mice, Rep7d: $n = 9$ eyes from 5 mice), central and peripheral ($n = 6$ eyes from 3 mice for each group) retina in (C). Within $1000 \mu\text{m}$ of the optic nerve defined as the central retina. **E** Quantification of the percentage reduction in RGC relative to the sham group in (D). Each data point in the bar graph represents one eye. Data were displayed as mean \pm SEM. * $p < 0.05$, ** $p < 0.01$, *** $p < 0.001$.

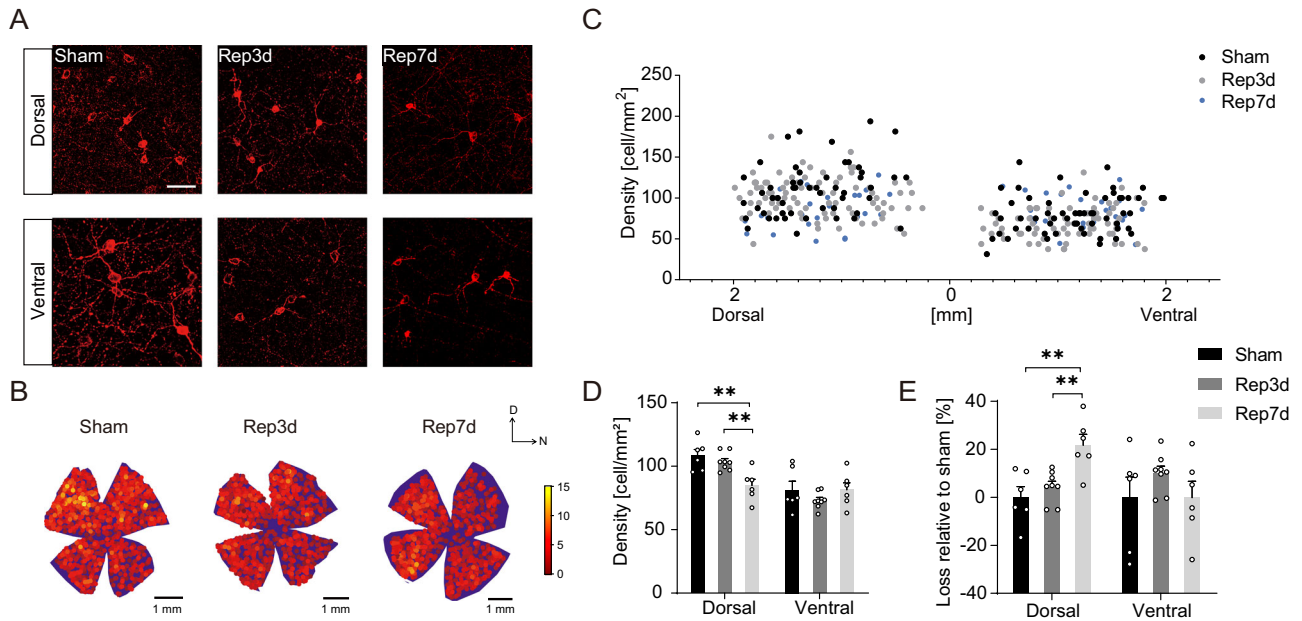


Fig. 4 | ipRGC is more tolerant after I/R. **A** Representative images for the cell counting of melanopsin expression (red) within the whole retina showing sham, 3 and 7 days after I/R injury. Scale bar: 50 μm . **B** Densities of ipRGCs across the whole retina. Color bar: number of cells/0.1 mm^2 . **D**: dorsal, **N**: nasal. **C** Scatter plots illustrating Mela+ cell density along the dorsal-ventral axis (horizontal axis with 0

for optic nerve). **D** Quantitative analysis of Mela+ cells density in the dorsal and ventral (Sham: $n = 6$ eyes from 3 mice, Rep3d: $n = 8$ eyes from 4 mice, Rep7d: $n = 6$ eyes from 3 mice) retina in **(C)**. **E** Quantification of the percentage reduction in RGC relative to the sham group in **(D)**. Each data point in the bar graph represents one eye. Data were displayed as mean \pm SEM. ****** $p < 0.01$.

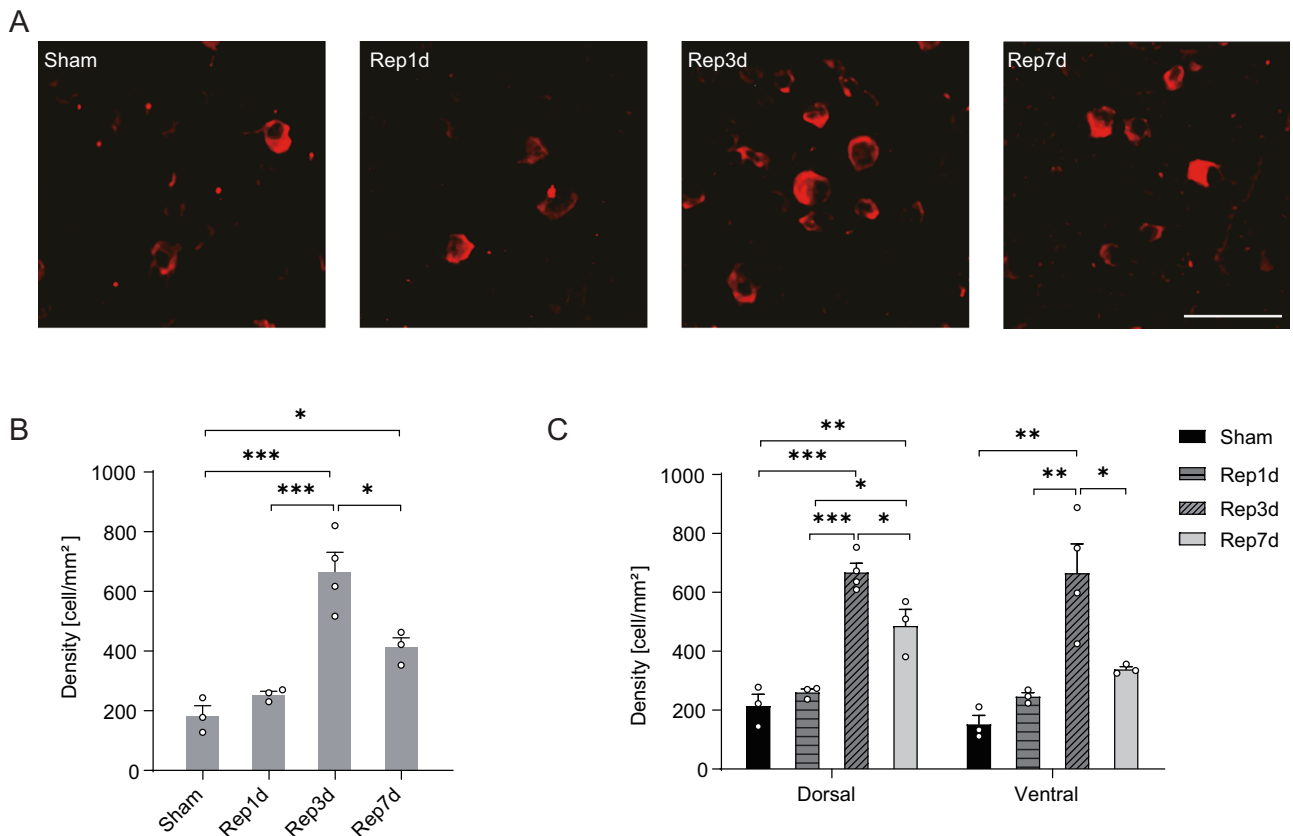


Fig. 5 | I/R activates mTOR in the retina. **A** Whole-mounted retinas from normal mice and 1 d, 3 d, and 7 d after ischemia, stained with pS6. Scale bar: 50 μm . **B**, **C** Quantification of the density of pS6+ cells in the whole retina (**B**) or dorsal and

ventral retina (**C**). Sham: $n = 3$ eyes from 3 mice; Rep1d: $n = 3$ eyes from 3 mice; Rep3d: $n = 4$ eyes from 4 mice; Rep7d: $n = 3$ eyes from 3 mice. Data were displayed as mean \pm SEM. ***** $p < 0.05$, ****** $p < 0.01$, ******* $p < 0.001$.

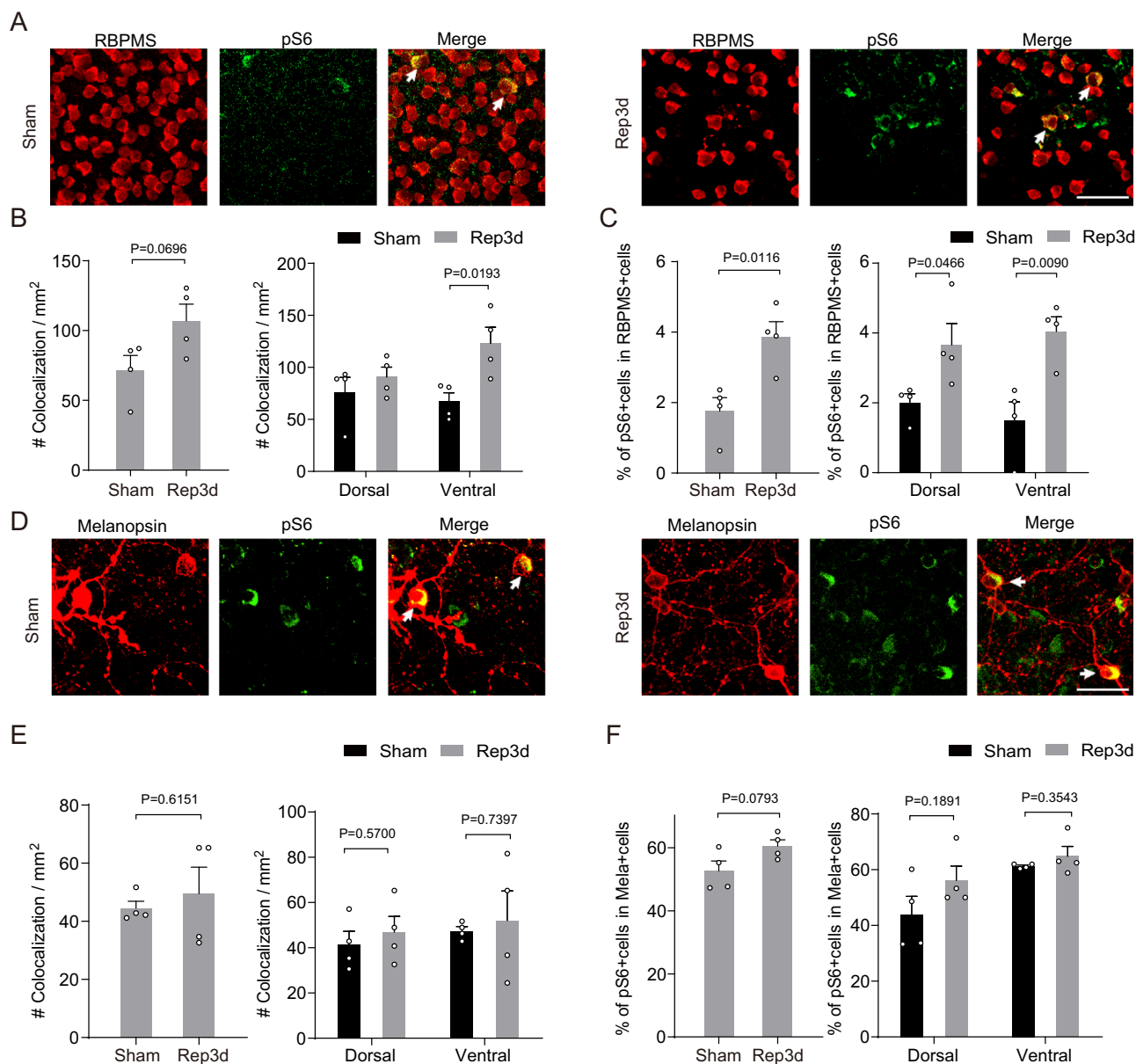


Fig. 6 | Differential mTOR activation in total RGCs and ipRGCs after I/R. **A** Exemplary images showing RBPMS (red) and pS6 (green) immunostaining in whole-mounted retinas. Arrows point to RBPMS+ cells expressing pS6. **B** Colocalization of pS6+ cells in RBPMS+ cells was analyzed for the whole retina (left) and local (dorsal and ventral) retina (right). **C** Percentage of RBPMS+ cells

expressing pS6 for the whole retina (left) and local (dorsal and ventral) retina (right). **D–F** The same as (A–C), but for the co-localization analysis between Mela+ cells and pS6+ cells. Scale bar: 50 μ m. *n* = 4 mice in each group. Data were displayed as mean \pm SEM. *P* values are shown in the figure.

Next, we assessed the changes in RGC number after the rapamycin application. The RBPMS and Brn3a staining showed that rapamycin administration decreased the total RGC and non-ipRGC loss, leading to a pronouncedly increased total RGC and non-ipRGC number in the I/R retinas (Fig. 8A, B; Supplementary Fig. 8). While for ipRGCs, the rapamycin administration did not protect them from I/R injury, with no significant difference in ipRGC density between retinas from mice with and without rapamycin administration (Fig. 8C, D), which might be due to the rapamycin-mediated decrease of mTOR activity in ipRGCs. Additionally, the overall protective effect of rapamycin on RGCs was associated with the restoration of visual function, as indicated by our visual cliff test data (Fig. 8E, F). Taken together, our rapamycin administration data showed that rapamycin selectively elevated mTOR activity in non-ipRGCs while suppressing overall mTOR in the inner retina. This elevation of mTOR activity was associated with reduced non-ipRGC loss and significant restoration of visual function.

Light modulates the protective effects of rapamycin on RGCs

RGCs receive and code various light information transmitted from the upper retinal circuits, requiring lots of energy that might aggravate ischemic injury. Therefore, we tested the idea that suppressing RGC activity by light deprivation might promote RGC survival and enhance the protective effects of rapamycin after I/R.

Before assessing the effect of light deprivation on RGC survival, we began our analysis in mTOR activity in total RGCs. We dark-adapted mice during the 3 days of reperfusion after ischemia. In the dark-adapted retinas, the expression of pS6 was strongly suppressed (Fig. 9A, B). Like normal light conditions, rapamycin strikingly inhibited the pS6 expression in the dark-adapted retinas (Fig. 9A, B). However, for the dark-adapted retinas, the decrease in pS6 expression did not exhibit in RGCs, with no significant difference in the number of pS6 expressed RGCs compared with normal light conditions (Fig. 9C–F). Actually, after light deprivation, the number of pS6 expressed RGCs comprised a larger fraction of the total pS6 expressed

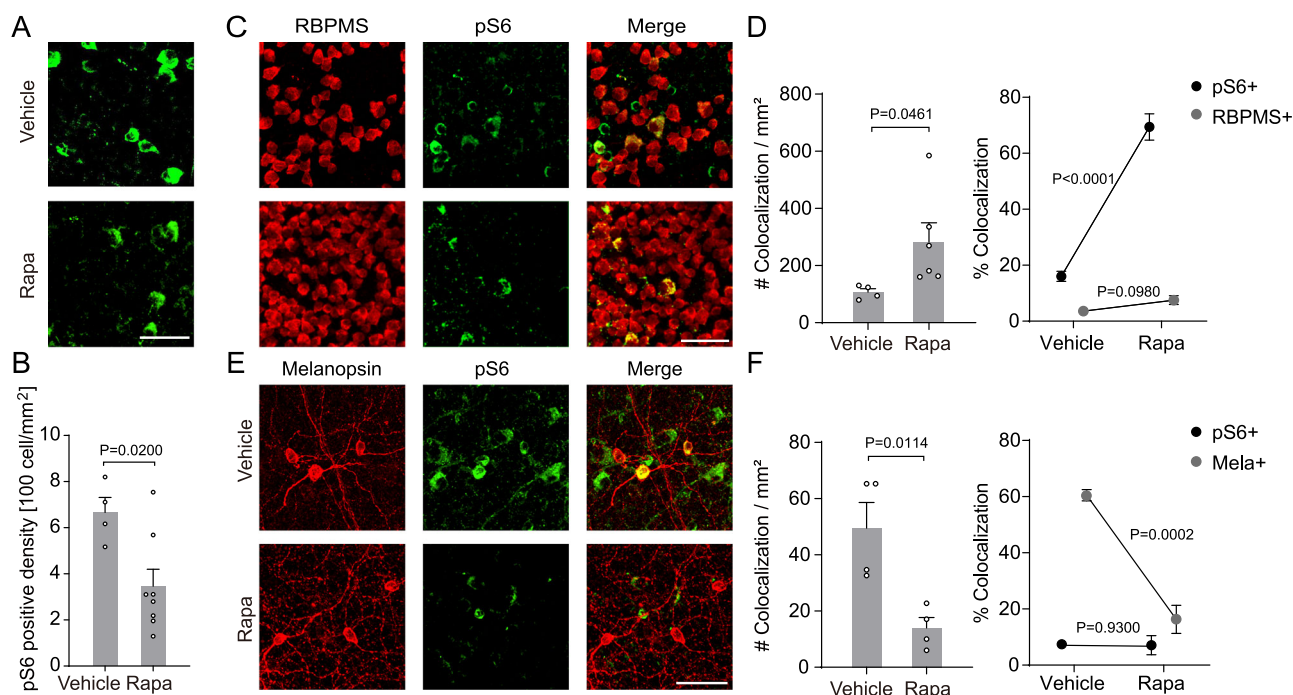


Fig. 7 | Rapamycin differentially affects mTOR activity in total RGCs and ipRGCs. **A** Immunostaining of pS6 in whole-mounted retinas from mice on the 3rd day of I/R injected with or without rapamycin (vehicle). Scale bar: 50 μ m. **B** Quantification of pS6 expressed cell density in the vehicle ($n = 4$ mice) and rapamycin ($n = 8$ mice) groups. **C** Images showing double labelling for RBPMS (red) and pS6 (green) from retinas with or without rapamycin. Scale bar: 50 μ m. **D** Left:

Density quantification of cells co-expressing pS6 and RBPMS in retinas; Right: Percentage of cells co-expressing pS6 and RBPMS relative to the total pS6+ cells and RBPMS+ cells. Vehicle: $n = 4$ mice; Rapa: $n = 6$ mice. **E** The same as **C**, but showing double labelling for melanopsin (red) and pS6 (green). Scale bar: 50 μ m. **F** As in (**D**) but for cells co-expressing pS6 and melanopsin. Vehicle: $n = 4$ mice; Rapa: $n = 4$ mice. Data were displayed as mean \pm SEM. *P* values are shown in the figure.

cells compared with retinas under normal light condition (Fig. 9E), indicating the decrease of pS6 expression induced by light deprivation might mainly occur in non-RGCs. Without light, the number of RGCs expressing pS6 was not changed by rapamycin administration (Fig. 9F), which was contrary to that under normal light, suggesting normal light stimulation is required for rapamycin to regulate mTOR activity in total RGCs after I/R.

We next determined whether light could affect the total RGC survival after I/R, and if light stimulation impaired rapamycin to protect total RGCs during I/R injury. Surprisingly, in I/R retinas, there was no significant difference in the RGC number between the dark-adapted retinas and retinas from mice under normal light conditions (Fig. 9G, H), suggesting normal light stimulation would not exacerbate the degeneration of RGCs. Additionally, though rapamycin decreased the total RGC loss after I/R under normal light, this protective effect was suppressed by light deprivation, exhibiting no differences in total RGC number and total RGC loss between retinas from mice with and without rapamycin application (Fig. 9H).

Finally, we investigated whether light deprivation could promote the neuroprotective effects of rapamycin on ipRGCs in ischemic retinas. Although rapamycin reduced the number of pS6-expressing ipRGCs under normal light conditions, dark-adapted retinas exhibited marked retention of pS6 expressing ipRGCs with rapamycin application, comparable to those in non-ischemic retinas (Fig. 10A–C). This finding indicates that light deprivation negates rapamycin’s inhibitory effects on mTOR activity in ipRGCs. Furthermore, with light deprivation, the decrease in ipRGC density observed in the dorsal retina after seven days of I/R was significantly reversed by rapamycin administration (Fig. 10D, E).

Together, these data demonstrate that the rapamycin-mediated neuroprotection in both total RGCs and ipRGCs is modulated by light conditions. For the total RGCs, light deprivation inhibited the elevation of mTOR activity induced by rapamycin and meanwhile invalidated the protective effects of rapamycin on their survival. For ipRGCs, light deprivation eliminated the inhibition of mTOR activity induced by rapamycin and

potentiated the protective effects of rapamycin. The distinct effects of rapamycin on total RGCs and ipRGCs under the same light conditions reveal that differential regulation of mTOR underlies the unique ischemic vulnerability between non-ipRGCs and ipRGCs.

Discussion

In this study, we show that I/R impairs retinal blood vessel networks mainly in the inner retina, associated with a striking decrease in the number of total RGCs but much less in the ipRGCs. Our findings indicate that mTOR activity is a crucial factor for the differential susceptibility of RGCs to I/R injury. Targeting mTOR activity modification with rapamycin to protect RGCs during I/R, different light conditions are required for distinct RGC populations. Our results add to the growing evidence for cell-type-specific injuries and mTOR regulations after I/R, and point out the importance of neuronal activity and mTOR signaling in the pharmacological protection of RGCs, which together could better guide exploitations on the treatments of neurodegeneration after I/R.

Neurodegeneration induced by I/R has been extensively studied. However, due to the large diversity of cell-type specializations in their microenvironment and intrinsic cell properties, the impact of I/R injury on different cell types located in different regions remains largely unknown. Regarding the development of more efficient treatments for I/R injury, it is essential to know where and which cell types are most vulnerable and which are more resistant. For the highly layer-organized retina, different layers are very likely to undergo differential degeneration after I/R. In this study, our OCTA data show that the inner retina is more susceptible than the outer retina, which is consistent with the previous studies^{4,35}. Like in other injuries, ipRGCs present high resistance to I/R injury while the cell loss is striking for the total RGCs^{3,21–24}. The different susceptibility of I/R is associated with high mTOR activity in ipRGCs and low mTOR activity in total RGCs, indicating a different resistance to I/R and distinct mTOR activity between ipRGCs and non-ipRGCs, which is demonstrated by our analysis of cell density and pS6 expression in Brn3a RGCs.

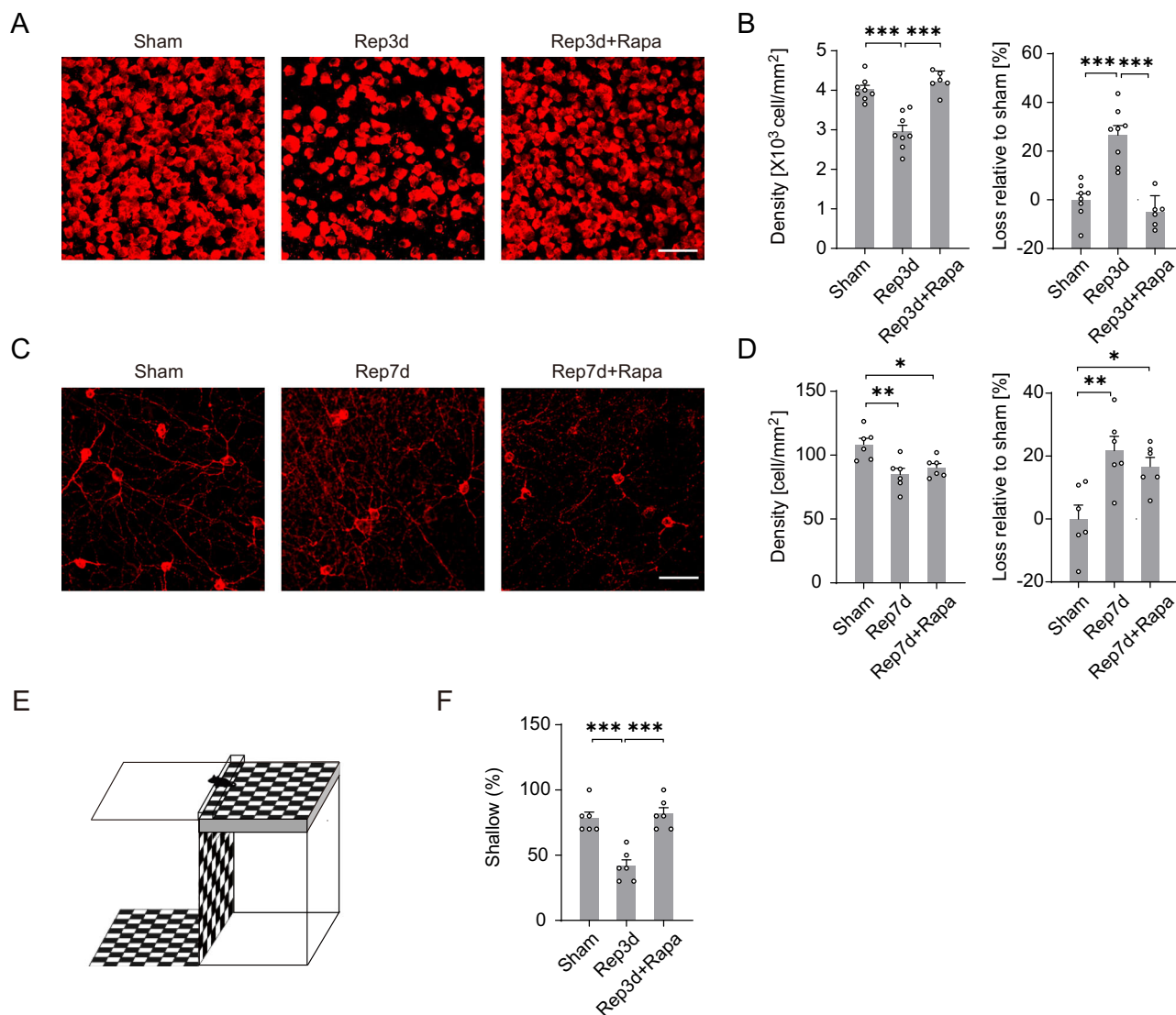


Fig. 8 | Rapamycin reduces cell loss in total RGCs after I/R. **A** Representative images of RBPMS+ cells in mice without I/R and mice with (Rep3d+Rapa) or without (Rep3d) rapamycin application. Scale bar: 50 μ m. **B** Left: Quantification of RBPMS+ cells in sham ($n = 8$ eyes from 4 mice), Rep3d ($n = 8$ eyes from 4 mice) and Rep3d+Rapa ($n = 6$ eyes from 3 mice) treated groups. Right: Quantification of the percentage reduction in RGCs relative to the sham group. **C, D** Similar to (A-B), but for dorsal Mela+ cell analysis at rep7d with different treatments ($n = 6$ eyes from 3

mice in each group). Scale bar: 50 μ m. **E** Schematic of visual cliff test. The component consists of a shallow end and a deep end for assessing depth perception. **F** Summary data of the performance in mice without I/R (sham) and after 3 days of I/R (Rep 3d) with and without rapamycin, $n = 6$ mice in each group. For each mouse, the percentage of shallow-side choices in 10 trials was measured. Data were displayed as mean \pm SEM. * $p < 0.05$, ** $p < 0.01$, *** $p < 0.001$.

Previous studies suggest that there are several mechanisms that can contribute to the high resistance of ipRGC to injuries. First, as dopamine has been reported to protect neurons from glutamate-induced death³⁶, dopamine amacrine cells can principally promote the survival of ipRGCs if they prefer to interact with ipRGCs. Second, the gene expression of ipRGCs makes them more resistant to injuries than other RGC types³⁷. Third, the type-specific distribution and subunit-combination of glutamate receptors can be involved in the differential susceptibility between RGC types^{38–40}. Here, our data suggest that high mTOR activity in ipRGCs contributes to their resistance to I/R injury. Compared with the total RGCs, ipRGCs present and maintain much higher mTOR activity before and after I/R, indicating sustained high mTOR signaling in ipRGCs during I/R accompanied with their high resistance, consistent with studies linking high mTOR activity to neuronal resistance after injury^{41–43}. Additionally, the protection effects of rapamycin on total RGCs are associated with elevated mTOR activity, and the abrogation of these protective effects is accompanied by no increase in mTOR activity. Furthermore, rapamycin

administration exhibits no protection on ipRGCs and strongly suppresses their mTOR activity under normal light conditions, while rapamycin promotes ipRGCs' survival and maintains their high mTOR activity under dark conditions. These findings suggest that mTOR activity is crucial for RGC survival after I/R. In the current belief, high mTOR activity is associated with low autophagy activity. Over-activation of autophagy has been shown to exacerbate the ischemic damage^{44–46}. Consistent with this notion, suppressing autophagy in global ischemia models decreases the damage^{46,47}. In this study, we show high mTOR activity is beneficial for the survival of RGCs, which is probably because of the low activation of autophagy in RGCs.

Rapamycin is the most commonly used inhibitor of mTOR and has been reported to alleviate neurodegeneration in pathological processes⁷. Although our data also demonstrate that rapamycin application in vivo decreases RGC loss and inhibits the total mTOR activity after I/R, we find that rapamycin application affects mTOR activity variously between different cell types. For ipRGCs, which are highly resistant to I/R injury, rapamycin inhibits mTOR activity. For

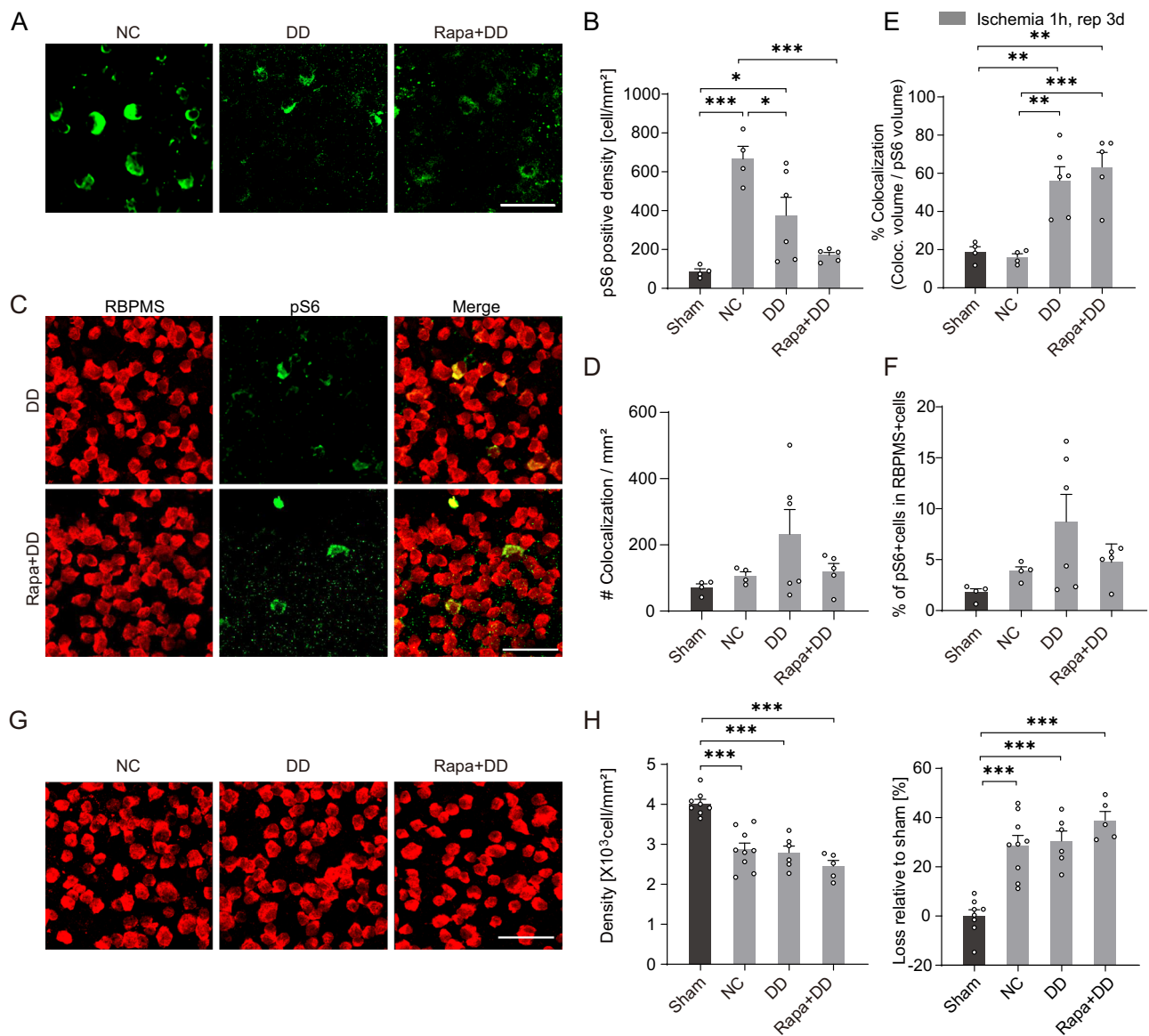


Fig. 9 | Dark adaptation invalidates the protective effect of rapamycin on total RGCs. **A** Exemplary images of pS6 staining in whole-mounted retinas from mice with different treatments. NC: Rep3d with normal 12:12 light-dark cycle; DD: Rep3d with 12:12 dark-dark cycle; Rapa+DD: Rep3d with rapamycin and 12:12 dark-dark cycle. Scale bar: 50 μ m. **B** Quantification of pS6 expressed cell density. **C** Images of the retinas from DD and Rapa+DD groups showing double labelling for RBPMS (red) and pS6 (green). Scale bar: 50 μ m. **D** Density of cells showing both pS6 and RBPMS positive signals. **E** The ratio of the co-localized cell number in (C) to the

corresponding pS6+ cell number. **F** Percentage of RBPMS+ cells that show pS6 positive signals. Sham: $n = 4$ mice; NC: $n = 4$ mice; DD: $n = 6$ mice; Rapa+DD: $n = 5$ mice for (B-F). **G** Representative images of RBPMS staining from mice treated with NC, DD and Rapa+DD. Scale bar: 50 μ m. **H** Left: Quantification of RBPMS+ cells. Right: Quantification of the percentage reduction in RGC relative to the sham group. (Sham: $n = 8$ eyes from 4 mice, NC: $n = 9$ eyes from 5 mice, DD: $n = 6$ eyes from 3 mice, Rapa+DD: $n = 5$ eyes from 3 mice). Data were displayed as mean \pm SEM. * $p < 0.05$, ** $p < 0.01$, *** $p < 0.001$.

the total RGCs, which show striking cell loss after I/R, rapamycin application activates mTOR. Along these lines, the suppression of total mTOR activity by rapamycin is very likely to occur in non-RGCs and most likely to be the glial cells. Indeed, our data show that in the I/R retinas, rapamycin suppresses mTOR activity in astrocytes and inhibits the I/R-induced increase in astrocyte number. This is consistent with the findings reported by a previous study, wherein rapamycin inhibits mTOR in astrocytes and decreases the activation of astrocytes after I/R, and meanwhile, reduces RGC loss¹⁵. It is highly probable that the functional modification of glial cells, together with the type-specific regulation of mTOR activity in RGCs, contributes to the protective effects of rapamycin on different RGC types. The distinct regulation of mTOR activity between glia and neurons, and even between different sub-types of neurons, can

largely increase the complexity of pharmacological treatments in vivo. Therefore, it is necessary to consider the cell-type specific effects when pharmacologically regulating mTOR and/or autophagy activities to protect neurons against ischemic injury. However, how to systematically regulate mTOR activity across different cell types to the level which is most beneficial for neurons is more challenging and needs further investigation.

For different ischemic cells, the main factors that lead to cell dysfunction and cell death are thought to be glutamate-induced excitotoxicity and intracellular Ca²⁺ overload¹⁴⁸⁻⁵⁰, which closely interact with and affect mTOR-related pathways^{9,51}. Regarding this, suppressing neuronal activity seems to be the cornerstone for neuronal protection following I/R injury. However, inhibiting neuronal activity has been demonstrated to increase neuronal apoptosis and

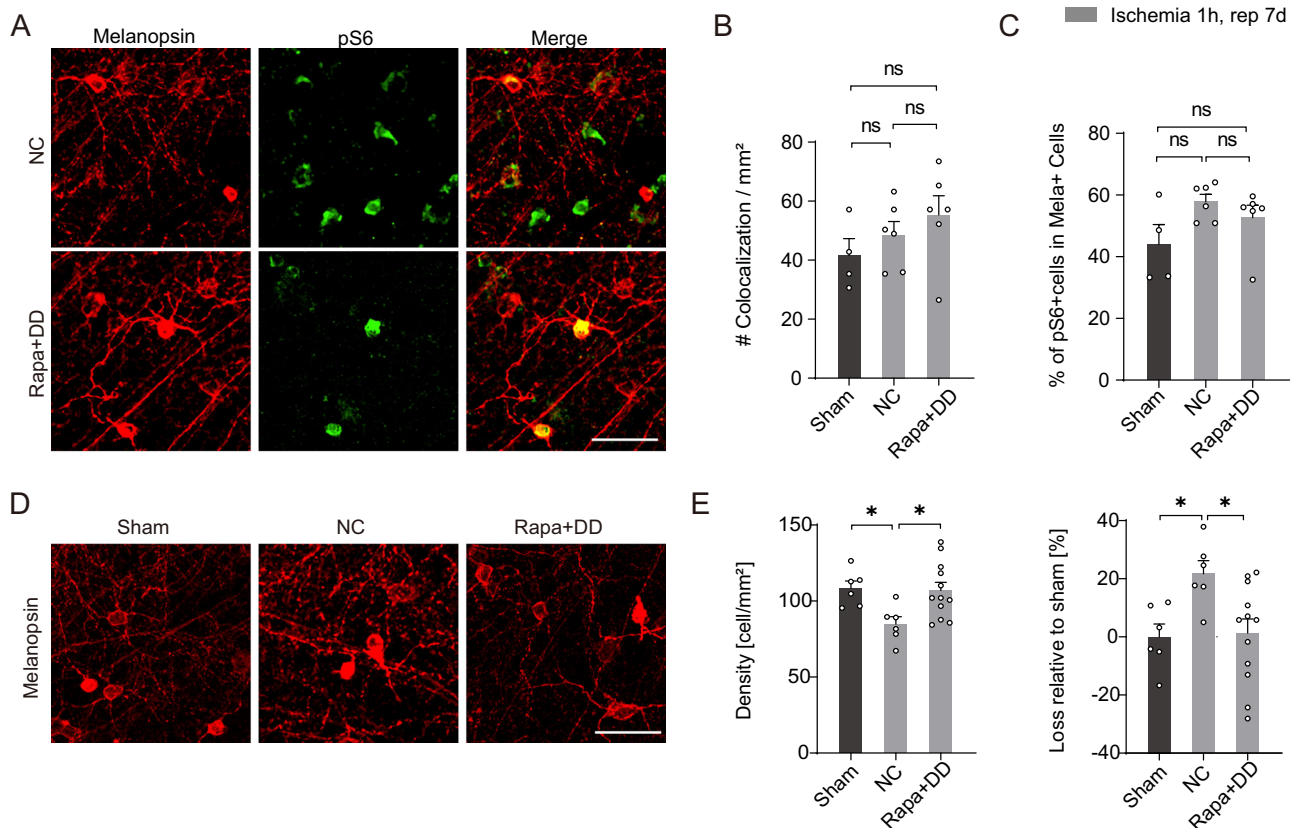


Fig. 10 | Light deprivation promotes the protective effect of rapamycin on ipRGCs. **A** Images of the dorsal retinas from mice treated with NC and Rapa+DD showing double labelling for Melanopsin (red) and pS6 (green). NC: Rep7d with normal 12:12 light-dark cycle; Rapa+DD: Rep7d with rapamycin and 12:12 dark-dark cycle. Scale bar: 50 μ m. **B** Density of cells showing both pS6 and melanopsin positive signals. **C** Percentage of Mela+ cells that show pS6 positive signals. Sham:

$n = 4$ mice; NC: $n = 6$ mice; Rapa+DD: $n = 6$ mice. Both eyes were used for (B, C). **D** Representative images of melanopsin staining for dorsal retinas in sham, NC and Rapa+DD groups. Scale bar: 50 μ m. **E** Left: Quantification of Mela+ cells. Right: Quantification of the percentage reduction in ipRGC relative to the sham group. (Sham: $n = 6$ eyes from 3 mice; NC: $n = 6$ eyes from 3 mice; Rapa+DD: $n = 12$ eyes from 6 mice). Data were displayed as mean \pm SEM. * $p < 0.05$, ns not significant.

decrease neuronal survival rate^{52,53}, while stimulating neurons after ischemia to increase neuronal activity improves their recovery and survival⁵⁴. Although we do not provide the retinal activity recordings, our data suggest that suppressing RGC activity via light deprivation does not promote RGC survival, at least does not alleviate the total RGC loss. When facilitating RGC survival via pharmacology, light conditions modulate the protective effects of pharmacology. For the total RGCs, light stimulation is essential for rapamycin to protect them from cell loss after I/R. Without light stimulation, despite rapamycin suppressing the overall mTOR activity like the normal light conditions, the total RGC loss is not alleviated, and the mTOR activity in total RGCs is not elevated. For ipRGCs, rapamycin shows protective effects with light deprivation. The requirement of different light conditions for pharmacological protection between total RGCs and ipRGCs seems to conflict when administrating pharmacology systematically. Notably, cell loss in ipRGCs occurs later than other RGCs after I/R injury, which allows us to determine the proper light conditions for the protection of specific RGC populations at distinct time windows after injury. Regarding different modulation of light on the neuroprotection of rapamycin between total RGCs and ipRGCs, many mechanisms can be involved. Our data suggest that one mechanism is probably their differential mTOR regulation. Here, the detailed impacts of light stimulation on the recovery of different RGC populations after I/R and the underlying mechanisms need further studies, probably via comprehensively investigating the morphological and functional alterations in different RGC types, the mTOR regulations and the corresponding glia activation states at various timepoints following I/R.

Materials and methods

Animals and the construction of I/R model

All studies were performed in accordance with the European Community guidelines for the use of experimental animals (2010/63/EU), approved by the Ethics Committee of Lanzhou University. Animal studies conformed to the Ethics Committee and Institutional Animal Care and Use Committee of Lanzhou University. Mice (C57BL/6 J) aged 8–12 weeks of either sex were used in this study. All mice were housed in animal facilities at Lanzhou University, with regular light conditions (12 h light/12 h dark cycle) at 22 ± 2 °C. Animals have free access to food and clean water. For fundus imaging, a total of 27 mice were allocated into 4 groups (Sham $n = 8$, Rep1d $n = 5$, Rep3d $n = 4$, Rep7d $n = 10$). For the analysis of RGC loss, 45 mice were employed (RBPMS + RGC: Sham $n = 5$, Rep1d $n = 4$, Rep3d $n = 7$, Rep7d $n = 5$; melanopsin+ RGCs: Sham $n = 3$, Rep3d $n = 4$, Rep7d $n = 3$; Brn3a+RGC: Sham $n = 7$, Rep3d $n = 7$). The analysis of pS6 expression and vessel density following I/R used one eye of the same batch of mice, respectively (Sham $n = 4$, Rep1d $n = 4$, Rep3d $n = 5$, Rep7d $n = 4$). To assess pS6 expression in RBPMS+ RGCs, melanopsin+ RGCs, Brn3a+ RGCs and astrocytes, 38 mice were used (8 for RBPMS+RGCs: Sham $n = 4$, Rep3d $n = 4$; 8 for melanopsin+ RGCs: Sham $n = 4$, Rep3d $n = 4$; 14 for Brn3a+RGCs: Sham $n = 7$, Rep3d $n = 7$; 8 for astrocytes: Sham $n = 4$, Rep3d $n = 4$). For rapamycin neuroprotection studies, 44 mice were used to evaluate rapamycin's effects on RGC survival under two conditions (with normal light: 6 for RBPMS + RGC at rep3d, 4 for melanopsin+ RGC at rep3d, 6 for melanopsin+ RGC at rep7d, 7 for Brn3a+RGC, 4 for astrocytes; with light deprivation: 11 for RBPMS + RGC at rep3d: DD $n = 6$, Rapa+DD: $n = 5$, 6 for melanopsin+ RGC at rep7d: Rapa+ DD: $n = 6$). Visual function preservation by rapamycin was evaluated in 18 mice (Sham $n = 6$,

Rep3d $n = 6$, Rep3d+Rapa $n = 6$). Data from retinas with pseudocataracts during OCTA scans or low OCTA imaging quality, and those distorted retinas during experiments were excluded from the dataset.

The BCAL model was adopted to induce I/R as previously described⁵⁵. First, mice were deeply anaesthetized by inhaling isoflurane (3%) and kept at an anaesthetized state by inhaling a lower concentration of isoflurane (0.5–1.5%). Then, the common carotid arteries of animals were carefully exposed in supine position and encircled with surgical sutures. After 1 h of ligation, the sutures were removed and the blood flow was re-perfused.

Fundus imaging

OCTA (isOCTA, Optoprobe, UK) was used to examine the changes in retinal blood perfusion in mice as described previously^{56–58}. At different time points during I/R, both pupils of anaesthetized mice were dilated with a single drop of Compound Tropicamide Eye Drops. Mice were properly placed to let the eye closely before the fundus camera and the corneal surface was perpendicular to the scan beam. For centering, the optic nerve head was used as a landmark. For each eye, one coronal image of the vascular network centred on the optic disc and one vertical image were acquired crossing through the center of the optic nerve. Using VesQuant, a built-in software in the OCTA imaging system, blood vessel densities at different retinal layers were analyzed, including the retinal nerve fiber layer (RNFL) together with ganglion cell layer (GCL), inner plexiform layer (IPL), and inner nuclear layer (INL). For the quantification of the thickness of different retinal layers, the thickness of the inner retinal layer (NFL + GCL + IPL), inner nuclear layer (INL), outer plexiform layer (OPL) and outer nuclear layer (ONL) were measured using octSegmentationGUI which built in the imaging system. The thickness of different layers within a horizontal distance of 300 μm starting at 200 μm away from the optic nerve head was measured.

Retina histochemistry

For retinal histochemistry, all animals were anaesthetized with pentobarbital sodium (100 mg/kg, i.p.) and perfused intracardially with 4% paraformaldehyde (PFA) followed by PBS. Their eyes were quickly marked at the dorsal side of the cornea and quickly enucleated. In 0.1 M PBS, retinas were oriented by a deep incising toward the optic nerve head and carefully isolated. Then retinas were cut into four wings and mounted on a filter paper (MF-MilliporeTM, 0.8 μm Black MCE, REF: AABPO2500). The retina together with the filter paper was transferred into a 24-well plate filled with 4% PFA for 20 min. Fixed retinas were washed 20 min \times 6 in 0.01 M PBS and incubated in blocking solution (10% normal donkey serum and 0.5% TritonX-100) at room temperature for 1 h. Next, retinas were incubated for 3 days at 4 $^{\circ}\text{C}$ with primary antibodies, followed by 20 min \times 6 in 0.01 M PBS washing and incubating with fluorescently labelled corresponding secondary antibodies for 2 h at room temperature in the dark. Finally, retinas were washed with 0.01 M PBS for 20 min \times 6 and mounted for imaging. The antibodies against the different markers included isolectin GS-IB4 Alexa Fluor 594 (1:600; Invitrogen, Cat: I-21413), rabbit RBPMS (1:400; GeneTex, Cat: GTX118619), mouse phosphorylated S6 ribosomal protein (pS6, 1:400, Cell Signaling, UniProt ID: #P62753), rabbit antibody to Brn3a (1:500; abcam, ab245230), rabbit antibody to GFAP (1:500; abcam; ab7260) and rabbit antibody to melanopsin (1:2000; Advanced Targeting Systems, Cat: AB-N39). The secondary antibodies included Alexa Fluor 594-conjugated goat anti-mouse IgG (H + L) (1:800; Invitrogen, Cat: A-11005), Alexa Fluor 594-conjugated goat anti-rabbit IgG (H + L) (1:800; Invitrogen, Cat: A-11012) and Alexa Fluor 488-conjugated goat anti-mouse IgG (H + L) (1:800; Invitrogen, Cat: A-11001).

Drug application

For blocking mTOR activity, rapamycin was supplemented in mice via i.p. injection (2 mg/kg) every other day, starting 1 day before ischemia.

Dark adaptation after ischemia

Mice were placed in a 24 h dark room immediately when the reperfusion started.

Confocal imaging

Fluorescent images of retinas were collected using a confocal microscope (Nikon AX R MP, made in Japan) with a 20 \times objective. Images were taken with a field of 1024 \times 1024 pixels at a z-step of 1 μm . For each wing, 2–3 fields (300 μm \times 300 μm) were imaged and a total 8–12 fields for each retina. The geometrical position of each scan area was saved and used for analyzing the relative position of the scan fields in the retina afterwards.

Visual cliff test

The visual cliff test was performed on a rectangular platform (56 cm \times 41 cm, length \times width). The platform contained a central ridge (3.0 cm height \times 3.4 cm width) that divided it into two sides. A checkered pattern was covered directly on the platform surface to create the shallow side. On the opposing side, a transparent glass sheet extended over an identical checkered pattern, creating a visual cliff of a 61-cm vertical drop beneath the glass. For each mouse, the percentage of trials in which the animal selected the shallow side was calculated (minimum 10 trials per subject).

Data analysis

OCTA imaging data: For OCTA imaging data, we first identified different retinal layers using the built-in software—ReconstructionUI (Optoprobe, UK) based on their layer-specific vessel network characters^{57,58}. NFL together with GCL was defined as the first 14 frames of the coronal image, IPL was defined as the 14 to 26 frames, and OPL was defined as the 26 to 40 frames to obtain the analyzed grey images. Bright pixels in the grey images indicate blood vessels. The images were imported into VesQuant for vascular network analysis. The threshold range is 0–1. Setting the threshold for the NFL + GCL vascular layer image at 0.6–0.75, the threshold for the IPL layer at 0.5–0.65, and the threshold for the OPL layer at 0.3–0.55 can optimally skeletonise the blood vessels. Automated vascular network analysis was then performed to obtain the percentage of vessel-positive pixels.

To measure retinal thickness in mice, the built-in software in OCTA imaging system (octSegmentationGUI, Optoprobe, UK) was used to analyze retinal vertical images. Firstly, the optic nerve region was removed from the vertical image, starting at 200 μm from the optic nerve, a region including all retinal layers with a width of 300 μm along the central to peripheral axis was drawn manually. Thickness measurements of the retina were made within this manually selected area. Then, the software automatically performed the delineation and segmentation of the layers in the selected region. Afterwards, we manually adjusted the automatic scribing part to ensure the accuracy of the recognition of different layers and obtained the thickness of each retinal layer. As shown in Fig. 1B, the average distance between the red and purple line segments is the thickness of the NFL, GCL and IPL layers; the average distance between the purple and white line segments is the thickness of the INL layer; the average distance between the white and cyan line segments is the thickness of the OPL layer; and the average distance between the cyan and yellow line segments is the thickness of the ONL layer.

Vessel density analysis based on IB4 staining: For the IB4-stained vessels, AngioTool software was used to measure the vessel density⁵⁹. For each image acquired from confocal microscope, the area with positive vessels was selected by adjusting the parameters in the software to obtain the contoured area of the vessel, and a convex hull formed by the vessel endpoints in the image was generated. The ratio of the area with positive vessels to the area of the convex hull was calculated as vessel density.

RGCs counting: Cell numbers were counted in a blinded fashion. The total RGC numbers were automatically counted using ImageJ. For this, imported images were first converted to “8-bit” format. The “Image-Adjust-Brightness/Contrast” module was employed to standardize image contrast, after stacking the 3D images to 2D, using the “Image-Adjust-Threshold” module to select signal-positive cells and convert them into binary images. After separating adjacent cells using the “Watershed” algorithm, automated cell counting was performed using the “Analyze Particles” module. For the melanopsin and GFAP positively labelled cells, we manually counted the cell numbers because of the massive dendritic labelling and relatively low cell

density. To relate the RGC density of each region to its retinal position, we calculated the linear distance from each photographic region to the optic nerve. The RGC loss rate was expressed as the ratio of the difference between the averaged RGC density without I/R and the RGC density of individual retinas after I/R to the averaged RGC density without I/R.

Determination of pS6 expressing cells: The number of pS6 expressing RGCs and astrocytes was determined using ImageJ based on the 3D confocal images. First, select ROIs for all RBPMS+ and pS6+ cells via a threshold setting. The pS6-expressing RGCs were then assessed by counting the intersections of RBPMS+ cell ROIs and pS6+ cell ROIs. Since the positive staining of pS6 surrounded the staining of Brn3a rather than colocalized, we manually counted the number of RGCs co-expressing Brn3a and pS6. The number of pS6 expressing ipRGCs and pS6 expressing astrocytes was also manually counted.

Topographic assessment of RGCs: After counting RGCs using ImageJ, the coordinates of each RGC in the retina were exported. The cell distribution was then analyzed in Igor Pro9.0 with a custom-written script. The RBPMS RGCs were calculated within each area of 60 × 60 μm² across the retina. The distribution of ipRGCs across the retina was determined by counting the number of ipRGCs within 0.1 mm² surrounding each ipRGC.

Statistics and Reproducibility

Two-tailed Student's t-test was used for comparisons between two groups. The rest of the data were analyzed using one-way ANOVA. Post hoc comparisons were carried out when a main effect showed statistical significance. All analysis was conducted by GraphPad Prism8. All data were presented as mean ± SEM. *P* value < 0.05 was considered to indicate statistical significance. **p* < 0.05, ***p* < 0.01, ****p* < 0.001, ns refers to no significant differences.

Reporting summary

Further information on research design is available in the Nature Portfolio Reporting Summary linked to this article.

Data availability

All data present in this study are available at <https://doi.org/10.5281/zenodo.15525108>.

Code availability

The custom scripts in Igor for generating the heatmaps of RGC distribution across the retina are available at <https://doi.org/10.5281/zenodo.15525108>.

Received: 14 November 2024; Accepted: 29 May 2025;

Published online: 11 June 2025

References

- Ruan, Y., Jiang, S., Musayeva, A. & Gericke, A. Oxidative stress and vascular dysfunction in the retina: therapeutic strategies. *Antioxidants* **9** (2020).
- Schmid, H., Renner, M., Dick, H. B. & Joachim, S. C. Loss of inner retinal neurons after retinal ischemia in rats. *Invest. Ophthalmol. Vis. Sci.* **55**, 2777–2787 (2014).
- Christensen, I. et al. The susceptibility of retinal ganglion cells to glutamatergic excitotoxicity is type-specific. *Front. Neurosci.* **13**, 1–14 (2019).
- Abcouwer, S. F. et al. Inflammatory resolution and vascular barrier restoration after retinal ischemia reperfusion injury. *J. Neuroinflammation* **18**, 186 (2021).
- Hwang, J.-Y. et al. Global ischemia induces lysosomal-mediated degradation of mTOR and activation of autophagy in hippocampal neurons destined to die. *Cell Death Differ.* **24**, 317–329 (2017).
- Villa-González, M., Martín-López, G. & Pérez-Álvarez, M. J. Dysregulation of mTOR signaling after brain ischemia. *Int. J. Mol. Sci.* **23**, (2022).
- Hadley, G. et al. Rapamycin in ischemic stroke: Old drug, new tricks?. *J. Cereb. Blood Flow. Metab.* **39**, 20–35 (2019).
- Kong, L. et al. Rapamycin alleviates mitochondrial dysfunction in anti-NMDAR encephalitis mice. *Int. Immunopharmacol.* **132**, 111910 (2024).
- Burket, J. A., Benson, A. D., Tang, A. H. & Deutsch, S. I. NMDA receptor activation regulates sociability by its effect on mTOR signaling activity. *Prog. Neuro-Psychopharmacol. Biol. Psychiatry* **60**, 60–65 (2015).
- Bar-Peled, L. & Sabatini, D. M. Regulation of mTORC1 by amino acids. *Trends Cell Biol.* **24**, 400–406 (2014).
- Zhang, Y. et al. Dichloromethane extraction from Piper nigrum L. and P. longum L. to mitigate ischemic stroke by activating the AKT/mTOR signaling pathway to suppress autophagy. *Brain Res.* **1749**, 147047 (2020).
- Wu, J. et al. Ecdysterones from Rhaponticum carthamoides (Willd.) Iljin reduce hippocampal excitotoxic cell loss and upregulate mTOR signaling in rats. *Fitoterapia* **119**, 158–167 (2017).
- Hou, Y. et al. Resveratrol provides neuroprotection by regulating the JAK2/STAT3/PI3K/AKT/mTOR pathway after stroke in rats. *Genes Dis.* **5**, 245–255 (2018).
- Yang, Y. et al. Arctium lappa L. roots ameliorates cerebral ischemia through inhibiting neuronal apoptosis and suppressing AMPK/mTOR-mediated autophagy. *Phytomedicine* **85**, 153526 (2021).
- Li, N. et al. Rapamycin mediates mTOR signaling in reactive astrocytes and reduces retinal ganglion cell loss. *Exp. Eye Res.* **176**, 10–19 (2018).
- Chauhan, A., Sharma, U., Jagannathan, N. R. & Gupta, Y. K. Rapamycin ameliorates brain metabolites alterations after transient focal ischemia in rats. *Eur. J. Pharmacol.* **757**, 28–33 (2015).
- Baden, T. et al. The functional diversity of retinal ganglion cells in the mouse. *Nature* **529**, 345–350 (2016).
- Bae, J. A. et al. Digital museum of retinal ganglion cells with dense anatomy and physiology. *Cell* **173**, 1293–1306.e19 (2018).
- Rheume, B. A. et al. Single cell transcriptome profiling of retinal ganglion cells identifies cellular subtypes. *Nat. Commun.* **9**, 1–1 (2018).
- Li, S. et al. Promoting axon regeneration in the adult CNS by modulation of the melanopsin/GPCR signaling. *Proc. Natl. Acad. Sci. USA* **113**, 1937–1942 (2016).
- Zhang, N., He, X., Xing, Y. & Yang, N. Differential susceptibility of retinal ganglion cell subtypes against neurodegenerative diseases. *Graefes Arch. Clin. Exp. Ophthalmol.* **260**, 1807–1821 (2022).
- Nadal-Nicolás, F. M., Sobrado-Calvo, P., Jiménez-López, M., Vidal-Sanz, M. & Agudo-Barriuso, M. Long-term effect of optic nerve axotomy on the retinal ganglion cell layer. *Invest. Ophthalmol. Vis. Sci.* **56**, 6095–6112 (2015).
- Vidal-Sanz, M. et al. Shared and differential retinal responses against optic nerve injury and ocular hypertension. *Front. Neurosci.* **11**, 235 (2017).
- La Morgia, C. et al. Melanopsin retinal ganglion cells are resistant to neurodegeneration in mitochondrial optic neuropathies. *Brain* **133**, 2426–2438 (2010).
- Rovere, G. et al. Melanopsin-containing or non-melanopsin-containing retinal ganglion cells response to acute ocular hypertension with or without brain-derived neurotrophic factor neuroprotection. *Invest. Ophthalmol. Vis. Sci.* **57**, 6652–6661 (2016).
- Honda, S. et al. Survival of alpha and intrinsically photosensitive retinal ganglion cells in NMDA-induced neurotoxicity and a mouse model of normal tension glaucoma. *Invest. Ophthalmol. Vis. Sci.* **60**, 3696–3707 (2019).
- Bleckert, A., Schwartz, G. W., Turner, M. H., Rieke, F. & Wong, R. O. L. Visual space is represented by nonmatching topographies of distinct mouse retinal ganglion cell types. *Curr. Biol.* **24**, 310–315 (2014).

28. Rizzi, M. et al. Lateral gain is impaired in macular degeneration and can be targeted to restore vision in mice. *Nat. Commun.* **13**, 2159 (2022).
29. Salinas-Navarro, M. et al. Retinal ganglion cell population in adult albino and pigmented mice: a computerized analysis of the entire population and its spatial distribution. *Vis. Res.* **49**, 637–647 (2009).
30. Hughes, S., Watson, T. S., Foster, R. G., Peirson, S. N. & Hankins, M. W. Nonuniform distribution and spectral tuning of photosensitive retinal ganglion cells of the mouse retina. *Curr. Biol.* **23**, 1696–1701 (2013).
31. Valiente-Soriano, F. J. et al. Distribution of melanopsin positive neurons in pigmented and albino mice: evidence for melanopsin interneurons in the mouse retina. *Front. Neuroanat.* **8**, 131 (2014).
32. Nadal-Nicolás, F. M. et al. Transient downregulation of melanopsin expression after retrograde tracing or optic nerve injury in adult rats. *Invest. Ophthalmol. Vis. Sci.* **56**, 4309–4323 (2015).
33. García-Ayuso, D. et al. Light-induced retinal degeneration causes a transient downregulation of melanopsin in the rat retina. *Exp. Eye Res.* **161**, 10–16 (2017).
34. Iwenofu, O. H. et al. Phospho-S6 ribosomal protein: A potential new predictive sarcoma marker for targeted mTOR therapy. *Mod. Pathol.* **21**, 231–237 (2008).
35. Palmhof, M. et al. From ganglion cell to photoreceptor layer: timeline of deterioration in a rat ischemia/reperfusion model. *Front. Cell. Neurosci.* **13**, (2019).
36. Vaarmann, A., Kovac, S., Holmström, K. M., Gandhi, S. & Abramov, A. Y. Dopamine protects neurons against glutamate-induced excitotoxicity. *Cell Death Dis.* **4**, e455 (2013).
37. Tran, N. M. et al. Single-cell profiles of retinal ganglion cells differing in resilience to injury reveal neuroprotective genes. *Neuron* **104**, 1039–1055.e12 (2019).
38. Bocconi, I. & Fairless, R. Retinal glutamate neurotransmission: from physiology to pathophysiological mechanisms of retinal ganglion cell degeneration. *Life* **12** (2022).
39. Li, Q., Jin, R., Zhang, S., Sun, X. & Wu, J. Group II metabotropic glutamate receptor agonist promotes retinal ganglion cell survival by reducing neuronal excitotoxicity in a rat chronic ocular hypertension model. *Neuropharmacology* **170**, 108016 (2020).
40. Sucher, N. J., Lipton, S. A. & Dreyer, E. B. Molecular basis of glutamate toxicity in retinal ganglion cells. *Vis. Res.* **37**, 3483–3493 (1997).
41. Agostinone, J. et al. Insulin signalling promotes dendrite and synapse regeneration and restores circuit function after axonal injury. *Brain* **141**, 1963–1980 (2018).
42. Saxena, S. et al. Neuroprotection through excitability and mTOR required in ALS motoneurons to delay disease and extend survival. *Neuron* **80**, 80–96 (2013).
43. Wang, P. et al. The mTOR cell signaling pathway is crucial to the long-term protective effects of ischemic postconditioning against stroke. *Neurosci. Lett.* **676**, 58–65 (2018).
44. Wei, N. et al. The involvement of autophagy pathway in exaggerated ischemic brain damage in diabetic mice. *CNS Neurosci. Ther.* **19**, 753–763 (2013).
45. Xu, Y., Tian, Y., Tian, Y., Li, X. & Zhao, P. Autophagy activation involved in hypoxic-ischemic brain injury induces cognitive and memory impairment in neonatal rats. *J. Neurochem.* **139**, 795–805 (2016).
46. Sun, D. et al. bFGF plays a neuroprotective role by suppressing excessive autophagy and apoptosis after transient global cerebral ischemia in rats. *Cell Death Dis.* **9**, 172 (2018).
47. Luo, C. et al. Poloxamer 188 attenuates cerebral hypoxia/ischemia injury in parallel with preventing mitochondrial membrane permeabilization and autophagic activation. *J. Mol. Neurosci.* **56**, 988–998 (2015).
48. Murphy, T. H., Li, P., Betts, K. & Liu, R. Two-photon imaging of stroke onset In Vivo Reveals That NMDA-receptor independent ischemic depolarization is the major cause of rapid reversible damage to dendrites and spines. *J. Neurosci.* **28**, 1756 LP–1751772 (2008).
49. Mao, R., Zong, N., Hu, Y., Chen, Y. & Xu, Y. Neuronal death mechanisms and therapeutic strategy in ischemic stroke. *Neurosci. Bull.* **38**, 1229–1247 (2022).
50. Neves, D., Salazar, I. L., Almeida, R. D. & Silva, R. M. Molecular mechanisms of ischemia and glutamate excitotoxicity. *Life Sci.* **328**, 121814 (2023).
51. Gong, R., Park, C. S., Abbassi, N. R. & Tang, S.-J. Roles of glutamate receptors and the mammalian target of rapamycin (mTOR) signaling pathway in activity-dependent dendritic protein synthesis in hippocampal neurons. *J. Biol. Chem.* **281**, 18802–18815 (2006).
52. Chen, X. et al. Treatment with enriched environment reduces neuronal apoptosis in the perinfarct cortex after cerebral ischemia/reperfusion injury. *Cell. Physiol. Biochem.* **41**, 1445–1456 (2017).
53. Young, D., Lawlor, P. A., Leone, P., Dragunow, M. & During, M. J. Environmental enrichment inhibits spontaneous apoptosis, prevents seizures and is neuroprotective. *Nat. Med.* **5**, 448–453 (1999).
54. Cheng, M. Y. et al. Optogenetic neuronal stimulation promotes functional recovery after stroke. *Proc. Natl. Acad. Sci. USA* **111**, 12913–12918 (2014).
55. Zhu, L. et al. Transient global cerebral ischemia induces rapid and sustained reorganization of synaptic structures. *J. Cereb. Blood Flow. Metab.* **37**, 2756–2767 (2017).
56. Liu, W., Luisi, J., Liu, H., Motamedi, M. & Zhang, W. OCT-angiography for non-invasive monitoring of neuronal and vascular structure in mouse retina: implication for characterization of retinal neurovascular coupling. *EC Ophthalmol.* **5**, 89–98 (2017).
57. Ferguson, L. R., Dominguez, J. M. II, Balaiya, S., Grover, S. & Chalam, K. V. Retinal thickness normative data in wild-type mice using customized miniature SD-OCT. *PLoS ONE* **8**, e67265 (2013).
58. Zhao, B., Ni, Y., Zhang, H., Zhao, Y. & Li, L. Endothelial deletion of TBK1 contributes to BRB dysfunction via CXCR4 phosphorylation suppression. *Cell Death Discov.* **8**, 429 (2022).
59. Zudaire, E., Gambardella, L., Kurcz, C. & Vermeren, S. A computational tool for quantitative analysis of vascular networks. *PLoS ONE* **6**, e27385 (2011).

Acknowledgements

We thank New Medical Science Innovation Platform of Lanzhou University for providing instrument support. This work was funded by the National Natural Science Foundation of China (No.32200810), the “Double First-Class” Research Start-up Funds of Lanzhou University (561120203), and Gansu Medical Products Administration Drug Research Project (Science and Technology) in 2022 (No.2022GSMPA007).

Author contributions

M.Z.: Writing—original draft, Methodology, Investigation, Formal analysis, Data curation, Conceptualization. Y.W.: Writing—review & editing, Methodology, Data curation. H.G.: Writing—review & editing, Methodology, Data curation. F.Q.: Writing—review & editing, Methodology, Investigation. X.Z.: Writing—review & editing, Supervision, Funding acquisition. Y.R.: Writing—original draft, Investigation, Visualization, Supervision, Conceptualization, Funding acquisition.

Competing interests

The authors declare no competing interests.

Ethics statement

The animal study protocol was approved by the Institutional Ethics Committee of the School of Basic Medical Sciences, Lanzhou University (protocol code jcyxy20220311, 15 March 2022).

Additional information

Supplementary information The online version contains supplementary material available at <https://doi.org/10.1038/s42003-025-08314-2>.

Correspondence and requests for materials should be addressed to Yanli Ran.

Peer review information *Communications Biology* thanks Francisco Valiente-Soriano and the other, anonymous, reviewer(s) for their contribution to the peer review of this work. Primary Handling Editor: Benjamin Bessieres. A peer review file is available.

Reprints and permissions information is available at <http://www.nature.com/reprints>

Publisher's note Springer Nature remains neutral with regard to jurisdictional claims in published maps and institutional affiliations.

Open Access This article is licensed under a Creative Commons Attribution-NonCommercial-NoDerivatives 4.0 International License, which permits any non-commercial use, sharing, distribution and reproduction in any medium or format, as long as you give appropriate credit to the original author(s) and the source, provide a link to the Creative Commons licence, and indicate if you modified the licensed material. You do not have permission under this licence to share adapted material derived from this article or parts of it. The images or other third party material in this article are included in the article's Creative Commons licence, unless indicated otherwise in a credit line to the material. If material is not included in the article's Creative Commons licence and your intended use is not permitted by statutory regulation or exceeds the permitted use, you will need to obtain permission directly from the copyright holder. To view a copy of this licence, visit <http://creativecommons.org/licenses/by-nc-nd/4.0/>.

© The Author(s) 2025